THE JOURNAL OF BIOLOGICAL CHEMISTRY VOL. 291, NO. 38, pp. 20220–20231, September 16, 2016

An ATP Binding Cassette Transporter Mediates the Uptake of α-(1,6)-Linked Dietary Oligosaccharides in *Bifidobacterium* and Correlates with Competitive Growth on These Substrates*

Received for publication, July 3, 2016 Published, JBC Papers in Press, August 8, 2016, DOI 10.1074/jbc.M116.746529

Morten Ejby[‡], Folmer Fredslund[§], Joakim Mark Andersen[‡], Andreja Vujičić Žagar[¶1], Jonas Rosager Henriksen[‖], Thomas Lars Andersen[**], Birte Svensson[‡], Dirk Jan Slotboom[¶1], and Maher Abou Hachem[‡2]

From the [‡]Protein Glycoscience and Biotechnology, Department of Bioengineering, Elektrovej, Building 375, [‖]Department of Chemistry, Kemitorvet Building 206, and [**]Department of Microtechnology and Nanotechnology, Produktionstorvet Building 423, Technical University of Denmark, DK-2800 Kgs. Lyngby, Denmark, [§]MaxLab, MAX IV Laboratory, Lund University, Ole Römers väg 1, 221 00 LUND, Sweden, and [¶]Membrane Enzymology, Institute for Biomolecular Sciences and Biotechnology, Rijksuniversiteit Groningen, Nijenborgh 4, 9747 AG Groningen, The Netherlands

The molecular details and impact of oligosaccharide uptake by distinct human gut microbiota (HGM) are currently not well understood. Non-digestible dietary galacto- and gluco-α-(1,6)-oligosaccharides from legumes and starch, respectively, are preferentially fermented by mainly bifidobacteria and lactobacilli in the human gut. Here we show that the solute binding protein (*Bl*G16BP) associated with an ATP binding cassette (ABC) transporter from the probiotic *Bifidobacterium animalis* subsp. *lactis* Bl-04 binds α-(1,6)-linked glucosides and galactosides of varying size, linkage, and monosaccharide composition with preference for the trisaccharides raffinose and panose. This preference is also reflected in the α-(1,6)-galactoside uptake profile of the bacterium. Structures of *Bl*G16BP in complex with raffinose and panose revealed the basis for the remarkable ligand binding plasticity of *Bl*G16BP, which recognizes the non-reducing α-(1,6)-diglycoside in its ligands. *Bl*G16BP homologues occur predominantly in bifidobacteria and a few Firmicutes but lack in other HGMs. Among seven bifidobacterial taxa, only those possessing this transporter displayed growth on α-(1,6)-glycosides. Competition assays revealed that the dominant HGM commensal *Bacteroides ovatus* was out-competed by *B. animalis* subsp. *lactis* Bl-04 in mixed cultures growing on raffinose, the preferred ligand for the *Bl*G16BP. By comparison, *B. ovatus* mono-cultures grew very efficiently on this trisaccharide. These findings suggest that the ABC-mediated uptake of raffinose provides an important competitive advantage, particularly against dominant *Bacteroides* that lack glycan-specific ABC-transporters. This novel insight highlights the role of glycan transport in defining the metabolic specialization of gut bacteria.

The gastrointestinal tract hosts a highly diverse microbial community referred to as the human gut microbiota (HGM)[3] (1). This community, which is established shortly after birth, develops rapidly to form one of the most densely populated ecological niches in nature by the age of 2–3 years. Despite millions of years of co-evolution with mammalian hosts (2), only recently has the profound impact of the gut microbiota on various aspects of human health, including metabolic and immune-disorders, colon cancer, and brain function, as well as rate of aging been established (3–5). Evidence is rapidly accumulating that advantage can be taken of the gut microbiota in diagnosis, treatment, and prevention of diseases and disorders. To realize this potential it is important to discern the complex metabolic interactions among different microbiota taxa, which promote a healthy composition and prevent imbalance (dysbiosis) associated with disease (6). Diet is a key effector of the composition of the HGM (7, 8), and the metabolism of glycans has been highlighted as pivotal in maintaining a healthy bacterial community (9). Raffinose family oligosaccharides (RFOs), containing α-(1,6)-galactosides (10), are abundant in soybeans and other legumes and seeds (11, 12), but are non-digestible by humans. Similarly, isomalto-oligosaccharides (IMOs), comprising α-(1,6)-gluco-oligosaccharides derived from breakdown of starch and the bacterial exopolysaccharide dextran (13, 14), are resistant to degradation by human digestive enzymes. Both of these classes of α-(1,6)-oligosaccharides selectively

* This work was supported by the Danish Strategic Research Council, the FøSu committee to the project "Gene discovery and molecular interactions in pre/probiotics systems, Focus on carbohydrate prebiotics"; Danish Research Council for Independent Research Natural Sciences (Grant 4002-00297) and the Biacore T100 instrument; the Carlsberg Foundation for isothermal titration calorimetry equipment (2011-01-0598); Ph.D. stipends from the Technical University of Denmark (to M. E. and J. M. A.). The authors declare that they have no conflicts of interest with the contents of this article.

The atomic coordinates and structure factors (codes 4ZS9, 4ZZE, and 4ZZA) have been deposited in the Protein Data Bank (http://wwpdb.org/).

[1] Supported by European Research Council starting grant (to D. J. S.), the EDICT program, and the Netherlands Organisation for Scientific Research (NWO).

[2] To whom correspondence should be addressed: Protein Glycoscience and Biotechnology, Dept. of Bioengineering, Technical University of Denmark, Elektrovej, Bldg. 375, DK-2800 Kgs. Lyngby, Denmark. Tel.: 45-45252732; 45-45252731; Fax: 45-45886307; E-mail: maha@bio.dtu.dk.

[3] The abbreviations used are: HGM, human gut microbiota; ABC, ATP binding cassette; *Bl*G16BP, *B. lactis* glycoside α-1,6 binding protein; IMO, isomalto-oligosaccharides; ITC, isothermal titration calorimetry; RFO, raffinose family oligosaccharides; SBP, solute binding protein; SPR, surface plasmon resonance; PDB, Protein Data Bank; r.m.s.(d.), root mean square (deviation).

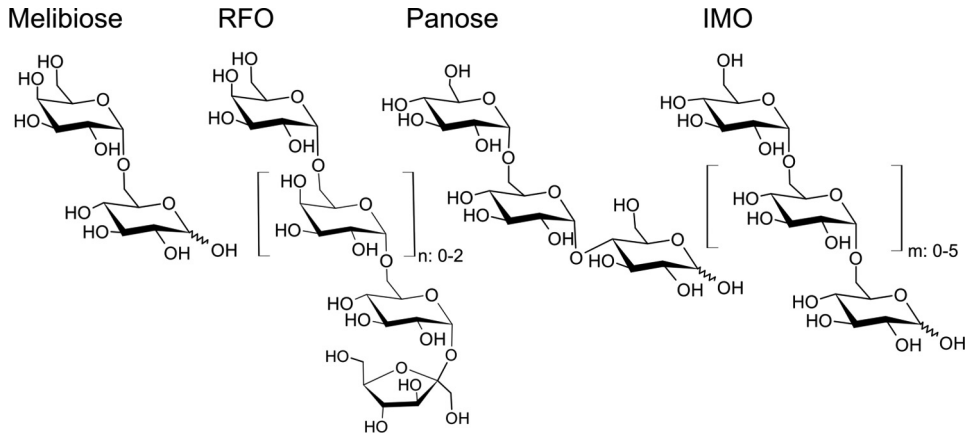

FIGURE 1. **Chemical structures of the oligosaccharide ligands of *Bl*G16PB.** RFOs, α-(1,6)-galactosides: $n = 0$, raffinose; $n = 1$, stachyose; $n = 2$, verbascose; IMOs, α-(1,6)-glucosides): $m = 0$, isomaltose; $m = 1$, isomaltotriose through to $m = 5$, isomaltoheptaose.

boost the counts of bifidobacteria and gut-adapted lactobacilli *in vitro* and *in vivo* (10, 15), but the molecular basis of this preferential enumeration is unclear.

Bifidobacteria are strictly saccharolytic, but in contrast to other commensals of the HGM most of their glycoside hydrolases are intracellular, and their genomes encode only a few extracellular hydrolases targeting polysaccharides (16, 17). Instead, bifidobacteria rely on their specialized carbohydrate transport systems for uptake of available oligosaccharides (18). ABC transporters are the most common class of glycan transporters in bifidobacteria (19). ABC transporters use the free energy of ATP hydrolysis via two intracellular nucleotide binding domains to energize the uptake of a variety of molecules. Extracellular solute binding proteins (SBPs) are responsible for capture of ligands, which are subsequently translocated through a pore formed by two transmembrane domains (20). Although some substrate recognition is conferred by the transmembrane domains, SBPs largely define the specificity and the affinity of bacterial ABC importers (21). Oligosaccharide transporters are likely to play a pivotal role in the highly competitive and extremely densely populated gut niche, as the intracellular (or periplasmic) accumulation of oligosaccharides precludes loss to competing organisms. Despite their importance, molecular insight for most oligosaccharide transporters in the gut niche and especially those from bifidobacteria is lacking.

Growth of the probiotic bacterium *Bifidobacterium animalis* subsp. *lactis* Bl-04 on the α-(1,6)-galactosides melibiose, raffinose, and stachyose and the α-(1,6)-glucosides isomaltose and panose (Fig. 1) differentially induced the expression of a locus encoding three glycoside hydrolases and an ABC transporter (22). In the present study, we determined the affinities of *Bl*G16BP and the SBP associated to this ABC transporter to a range of α-(1,6)-oligosaccharides and established its specificity for galactosides and glucosides sharing a common α-(1,6)-diglycoside motif. The structures of the SBP in complex with the two preferred ligands raffinose and panose provided insight into the structural basis for this specificity. Genetic and phylogenetic analyses show that close homologues of *Bl*G16BP are conserved within most bifidobacteria and a few strains of Firmicutes, consistent with preferential fermentation of α-(1,6)-oligosaccharides by these taxonomic groups of the HGM. Competition assays between *B. ovatus*, from the dominant HGM genus *Bacteroides*, and *B. animalis* subsp. *lactis* provided evidence that ABC-mediated oligosaccharide uptake confers an advantage in competition for raffinose, the preferred carbohydrate ligand for the identified ABC transporter.

TABLE 1
Binding parameters of *Bl*G16BP measured by SPR

Carbohydrate	K_D [a]	R_{max} [b]	χ^2 [c]
	μm		
Melibiose	729 ± 70	24	0.22
Raffinose	21 ± 4	35	0.12
Stachyose	327 ± 11	37	0.27
Verbascose	>4000	55	0.38
Isomaltose	1060 ± 73	19	0.06
Isomaltotriose	126 ± 3	33	0.70
Panose	9 ± 0	35	0.11
Isomaltotetraose	94 ± 1	42	0.05
Isomaltopentaose	103 ± 1	51	0.07
Isomaltohexaose	104 ± 1	56	0.06
Isomaltoheptaose	143 ± 1	69	0.04

[a] Dissociation constants (K_D) are the means of triplicates with the S.E.
[b] The maximum binding level from the fits to a one-binding-site model.
[c] χ^2, statistical goodness of the fit to a one-site-binding model.

This first biochemical and structural study of an α-(1,6)-oligosaccharide transport protein presented here provides a basic understanding of the versatility of ABC transporter associated SBPs in glycan capture and provides evidence for a competitive advantage associated with ABC-mediated glycan transport.

Results

BlG16BP Displays Dual Specificity to α-(1,6) Galactosides and Glucosides—Ligand preference of *Bl*G16BP was explored using SPR. No binding to the monosaccharides fructose, galactose, and glucose was observed. The SBP was specific for α-(1,6)-glucosides (IMO and panose) and α-(1,6)-galactosides (RFO) (Fig. 1) as judged by the lack of binding to the β-glycosides cellobiose, xylo-oligosaccharides, β-galacto-oligosaccharides, β-fructo-oligosaccharides, or malto-oligosaccharides. The binding kinetics rate constants were too fast to be modeled, and the equilibrium dissociation constants (Table 1) were determined from steady state sensograms (Fig. 2). The highest affinity was measured toward the trisaccharides panose and raffinose (Table 1) with K_D values of 9 μM and 21 μM, respectively. Reducing the ligand size to a disaccharide resulted in a

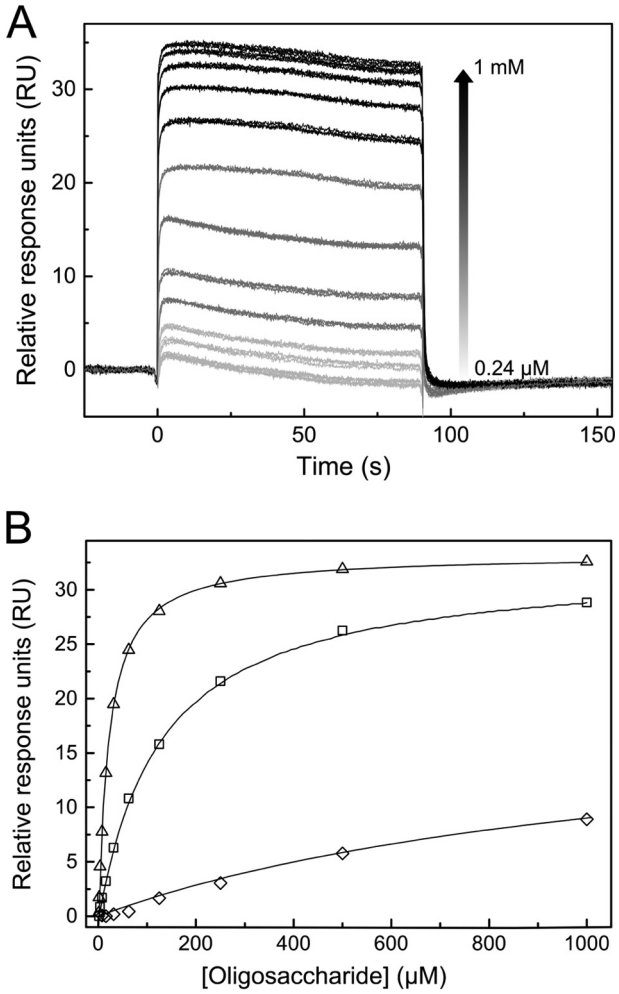

FIGURE 2. **Ligand binding to *Bl*G16BP as analyzed by surface plasmon resonance.** *A*, reference and baseline-corrected sensograms depicting binding of raffinose (0.24 μM-1 mM) to *Bl*G16BP at 25 °C. *B*, relative response as function of raffinose concentration (*triangles*), isomaltotriose (*squares*), and isomaltose (*diamonds*) and 1:1 binding model fits to the data (*solid lines*).

TABLE 2
Thermodynamic parameters of panose and raffinose binding to *Bl*G16BP measured by isothermal titration calorimetry

Oligosaccharide	K_D	ΔG	ΔH	$-T\Delta S$	n
	μm	*kJ/mol*	*kJ/mol*	*kJ/mol*	
Panose	17.5 ± 0.3	−27.1	−63.7 ± 0.5	36.5	0.70 ± 0.01
Raffinose	27 ± 2	−26.1	−46.3 ± 0.1	20.2	0.60 ± 0.02

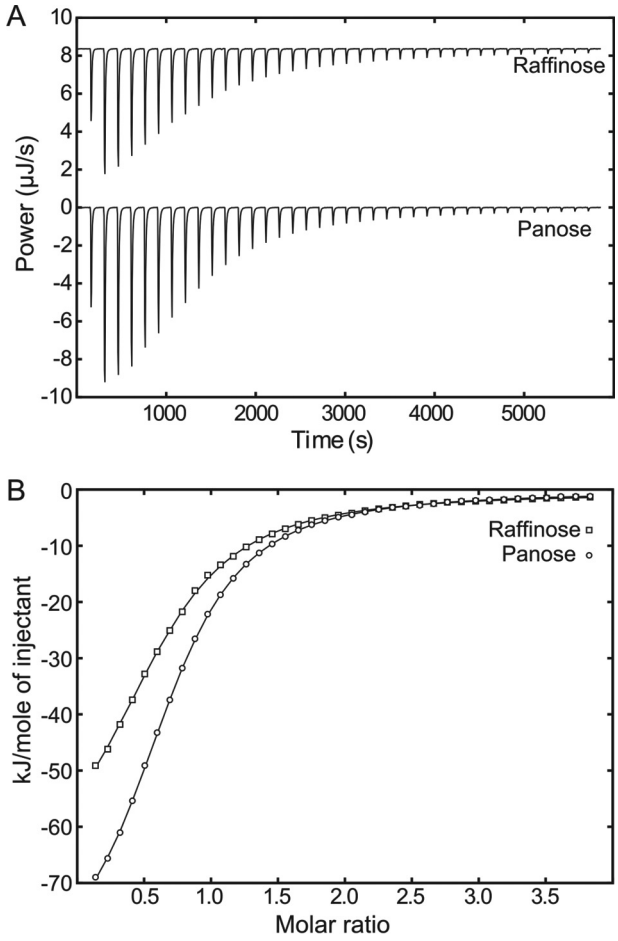

FIGURE 3. **Binding energetics of panose and raffinose to *Bl*G16BP analyzed by ITC.** *A*, representative heat traces of 2 mM panose and raffinose titrated into 108 μM *Bl*G16BP (see "Experimental Procedures"). *B*, integrated binding isotherms from *panel A* and single site binding model fits shown as *solid lines*. The experiments were performed at 25 °C in 20 mM citrate-phosphate buffer, pH 7.0.

substantial affinity reduction (~35-fold for the melibiose compared with raffinose and 120-fold for isomaltose as compared with panose). By contrast, the change in affinity with increasing oligosaccharide size was clearly different between the RFO and the IMO. Thus, the presence of two additional α-(1,6) galactosyl moieties at the non-reducing end of raffinose in verbascose abolished the binding within the tested ligand concentration range, whereas the affinity for the α-(1,6)-glucosides with a degree of polymerization of 3–7 was similar and only ~14-fold lower than for the preferred trisaccharide panose (Table 1). The binding affinity of *Bl*G16BP for raffinose was essentially unchanged in the pH range 5.5–8.0 (data not shown).

The thermodynamic parameters and binding stoichiometry for panose and raffinose were determined using isothermal titration calorimetry (ITC) and revealed a 1:1 binding driven by a favorable enthalpy change, which was offset by a large unfavorable binding entropy (Table 2 and Fig. 3). The affinity trend and the magnitude of the binding constants were in good agreement with the SPR data.

Overall Three-dimensional Structure—Crystal structures of *Bl*G16BP in complex with the two preferred ligands were solved to a maximum resolution of 1.4 Å (Table 3). *Bl*G16BP adopts a canonical SBP-fold (cluster B type SBP according to structural classification; Ref. 21), which comprises two domains of different size joined by a tripartite hinge region with the ligand binding site located at the domain interface (Fig. 4, A and *B*). Domain 1 (1–162; 327–373) is formed by six α-helices and five β-strands, two of which form a part of the hinge region and continue into the larger C-terminal domain (Domain 2). The loop spanning Ser-86 to Leu-93 in Domain 1 was not ordered, as judged by a poor electron density map, and no model is included for this region The unmodeled region corresponds to Pro-40–Phe-47 of the maltose-binding protein (MBP) from *Escherichia coli*, which is located at the interface between MBP and the transmembrane MalG domain in the pretranslocation state of the ABC-transporter (23). Domain 2 (167–322; 390–

TABLE 3
Data collection and refinement statistics of the complex structure of *Bl*G16BP with raffinose and panose and a selenomethionine derivative
Statistics were generated with MolProbity and Scala.

	*Bl*G16BP raffinose	*Bl*G16BP panose	*Bl*G16BP SeMet
PDB ID	**4ZS9**	**4ZZE**	**4ZZA**
Wavelength (Å)	0.9797	0.9773	0.9805
Resolution range (Å)	57-1.37 (1.41-1.37)	23-1.76 (1.82-1.76)	43.4-2.019 (2.091-2.019)
Space group	$P\,2_1\,2_1\,2_1$	$P\,2_1\,2_1\,2_1$	$P\,2_1\,2_1\,2_1$
Unit cell (Å)	55.54 90.82 146.75	54.88 91.33 142.05	55.39 90.95 145.53
Unique reflections[a]	151,108 (10,787)	70,949 (6,995)	48,992 (4,766)
Multiplicity[a]	6.2 (3.4)	3.4 (3.2)	4.1 (4.1)
Completeness (%)[a]	96.9 (94.1)	99 (99)	100 (99)
R-meas[a]	0.08 (0.775)	0.098 (0.764)	0.136 (0.477)
Mean I/σ(I)[a]	12.8 (2.1)	10.65 (2.12)	11.9 (3.53)
Wilson B-factor (Å^2)	13.3	17.7	14.0
R-factor	0.132	0.158	0.166
R-free	0.167	0.205	0.210
Number of atoms			
Macromolecules	6,030	6,031	5,767
Ligands	87	81	68
Water	1,114	987	853
Protein residues			
r.m.s. bonds (Å)	0.013	0.005	0.012
r.m.s. angles (°)	1.35	0.97	1.26
Ramachandran favored (%)	98	98	98
Ramachandran outliers (%)	0	0	0
Clash score	1.66	2.32	2.28
Average B-factor (Å^2)	18.4	20.0	15
Macromolecules (Å^2)	16.3	18.6	14.1
Ligands (Å^2)	16.7	14.8	8.9
Water (Å^2)	30.0	29	22

[a] Values in the parentheses are for the highest resolution shell.

437) consists of 11 α-helices and 3 β-strands. The hinge region comprises two short β-strands arranged in an anti-parallel β-sheet spanning the two domains (163–166; 323–326) and the loop 372–375 (Fig. 4). A DALI structure comparison search (24) against the Protein Data Bank (PDB) identified the raffinose-binding protein RafE[4] from the *Streptococcus pneumoniae* (PDB code 2i58; Z-score = 39.0; r.m.s.d. = 2.5 Å for 363 aligned C_α atoms and 23% sequence identity) as the structurally most related orthologue to *Bl*G16BP. The second best hit is the arabinoxylo-oligosaccharide-specific SBP from the same organism (25) (PDB code 4c1u; Z-score = 37.0; r.m.s.d. = 2.4 Å for 354 aligned C_α atoms and 23% sequence identity).

Ligand Binding Site—The crystal structures of *Bl*G16BP in complex with raffinose and panose showed well defined densities for the bound oligosaccharides in the ligand binding site that features a deep but open pocket large enough to accommodate a trisaccharide. Three aromatic residues from Domain 2 provide stacking interactions to each glycosyl ring in a trisaccharide ligand, whereas polar contacts are provided by both domains of *Bl*G16BP. The non-reducing end glycosyl unit of both ligands (galactosyl in raffinose and glucosyl in panose) stacks onto Phe-392 (defined as position 1) and makes polar contacts to Asp-394, Asn-109, and His-395 (Fig. 4, *D* and *E*). Interestingly Asp-394 is able to form hydrogen bonds to both the equatorial C4-OH of the nonreducing end glucosyl in panose and the axial C4-OH of the galactosyl in raffinose, thus allowing for an equivalent mode of ligand binding at position 1 (Fig. 4, *D* and *E*). The glucosyl moiety of raffinose and panose at position 2 stacks onto Tyr-291 and makes polar contacts to Lys-58, Glu-60, and Asp-326. Although the pyranose rings at positions 1 and 2 can be overlaid almost perfectly, the planes of the terminal glycosyl moieties residues at position 3 are almost orthogonal to each other. Thus, the glucosyl moiety of panose stacks onto Trp-216 with almost parallel planes of the sugar ring and the indole side chain (Fig. 4, *D* and *E*). By contrast, the fructosyl residue in raffinose has a smaller area of van der Waals contact with Trp-216, with the planes of the furanose and indole rings being almost orthogonal to each other (Fig. 4, *D* and *E*).

Conservation of BlG16BP within Bifidobacterium—Homologues of *Bl*G16BP are encoded by genomes of several species within *Bifidobacterium*. While the solvent-exposed residues are variable, the binding pocket residues of *Bl*G16BP that make direct ligand contacts are invariant in *Bifidobacterium* (data not shown). An exception is the conservative substitution of Asn-109 to aspartic acid in some *Bifidobacterium longum* subsp. *longum* strains.

Genetic Organization and Phylogenetics of α-(1,6)-Galactoside/Glucoside-binding Proteins—The composition and conservation of loci encompassing orthologues of the *Bl*G16BP gene within *Bifidobacterium* was performed. Genes encoding permease components of an ABC importer, transcriptional regulators, GH36 α-galactosidases that mediate degradation of soybean α-1,6-galactosides (RFO), oligo-α-1,6-glucosidases (glycoside hydrolase family 13, subfamily 31, GH13_31) that catalyze the hydrolysis of α-(1,6)-glucosides (IMO), were invariably co-localized with *Bl*G16BP orthologues in human gut adapted taxa (Fig. 5). This organization defines the α-(1,6)-galactoside/glucoside utilization loci in *Bifidobacterium* with the exception of the insect gut-residing *Bifidobacterium asteroides* (Fig. 5).

The occurrence of potential ABC transporters of α-(1,6)-glycosides in other taxa, particularly from the gut niche, was analyzed using a different strategy to overcome the low sequence

[4] Substrate-binding protein component of the raffinose uptake system from *S. pneumonia*.

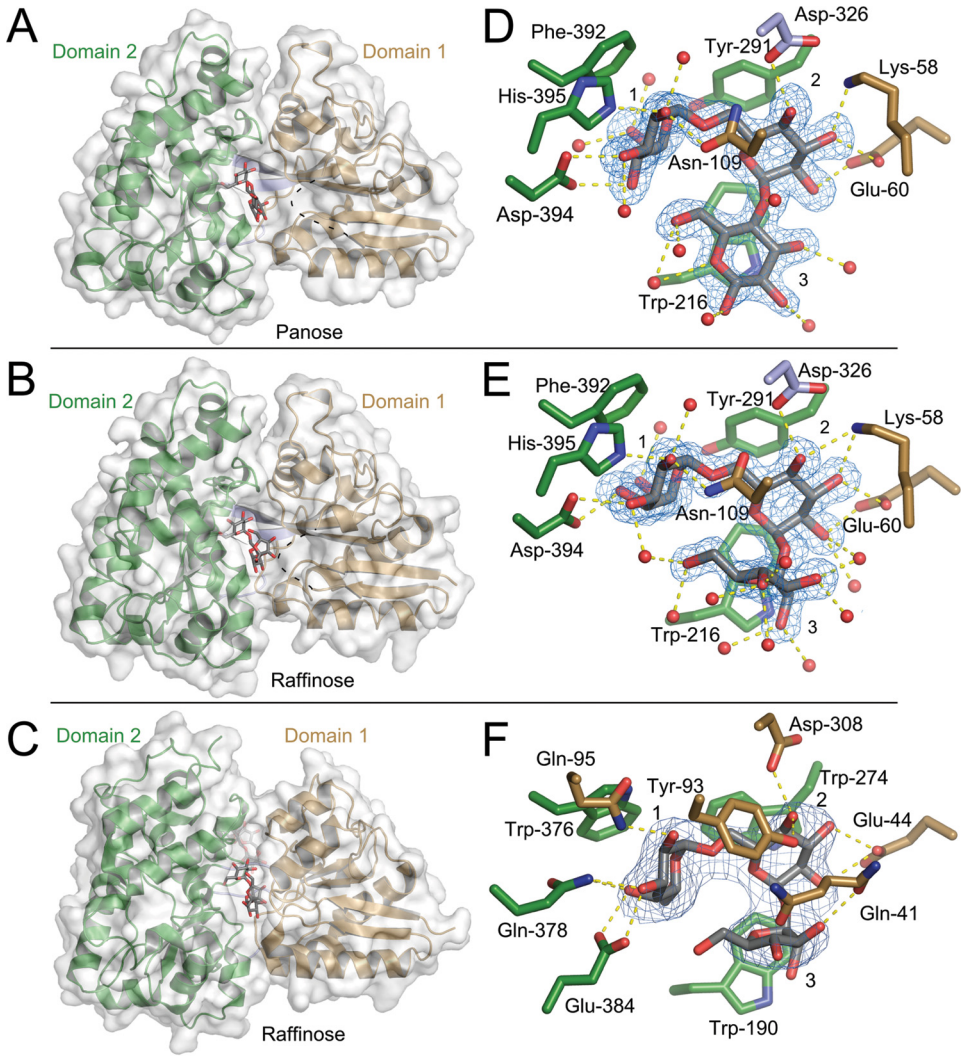

FIGURE 4. Shown is a ribbon representation of the overall structure of *Bl*G16BP in complex with panose (*A*) and raffinose (*B*) and the binding protein from *S. pneumoniae* TIGR4 (RafE, PDB code 2i58) in complex with raffinose (*C*). The SBPs consist of an N-terminal domain (Domain 1, *brown*) and a larger C-terminal domain (Domain 2, *green*). The two domains are linked by hinge regions shown in *light blue*. Shown is a close-up of the binding sites of *Bl*G16BP in complex with panose (*D*) and raffinose (*E*) and RafE in complex with raffinose (*F*), which is shown in a slightly tilted view compared with *D* and *E* for clarity. The *dashed black line* in *panels A* and *B* illustrates a flexible loop between residues Ser-86 and Leu-97, which could not be modeled due to missing electron density. A σA-weighted difference electron density map (coefficients $mF_{obs} - DF_{calc}$) was calculated without phase information from the ligand and contoured at 3σ as a *light blue mesh*. *Yellow dashes* depict polar interactions to protein atoms or water (*red spheres*). Polar interactions were identified with PyMOL using a threshold of 3.1 Å. Main chain atoms are omitted for clarity unless they participate in polar interactions.

conservation of SBPs. The genetic co-localization of an ABC transporter and an α-galactosidase of family GH36 was used as a discriminator to map the taxonomic distribution of *Bl*G16BP homologues in putative α-(1,6)-galactoside utilization loci. Using this approach, 263 gene loci encoding GH36 enzymes (mainly α-galactosidases) together with an ABC transporter and enzymes predicted to be involved in the degradation of α-(1,6)-glucosides (*e.g.* α-(1,6)-glucosidases of GH13_31) or the sucrose moieties produced from RFO (*e.g.* sucrose phosphorylases of GH13_18 or sucrose hydrolases of GH32) were found. Most of the loci originated from the Firmicutes and Actinobacteria, including bifidobacteria species and other taxa typically associated with human hosts (Fig. 5). These SBPs populated three subtrees (*1*, *2*, and *3*) in this phylogenetic analysis (Fig. 6). *Bl*G16BP and homologous sequences sharing the same genetic organization were in subtree 1. By contrast, subtree 2 SBPs co-localized with putative α-*N*-acetylgalactosaminidase genes (of GH36, data not shown), suggesting a role in uptake of α-*N*-acetyl-hexoseamine-containing glycans, *e.g.* from mucin. Subtree 3 is mostly populated by SBPs from marine or soil bacteria. The majority of bifidobacterial SBPs populate a single branch in subtree 1 together with *Bl*G16BP (Fig. 6). A few sequences from the HGM *Eubacterium rectale*, *Ruminococcus SR1/5*, and *Ruminococcus torques* spp. (26, 27), cluster on an adjacent branch to bifidobacterial counterparts (Fig. 6). Another clade of *Bl*G16BP homologues harbored sequences from acidophilus cluster lactobacilli (28), *e.g. Lactobacillus acidophilus* and *Lactobacillus crispatus* together with *Streptococcus* spp., *e.g. Streptococcus mutans,* a human oral cavity commensal (29).

Carbohydrate Uptake by B. animalis subsp. lactis Bl-04—To assay for oligosaccharide uptake preference, *B. animalis* subsp. *lactis* Bl-04 was grown in the presence of equal amounts of the RFOs melibiose, raffinose, and stachyose (Fig. 1). The depletion of oligosaccharides was monitored in the culture supernatant

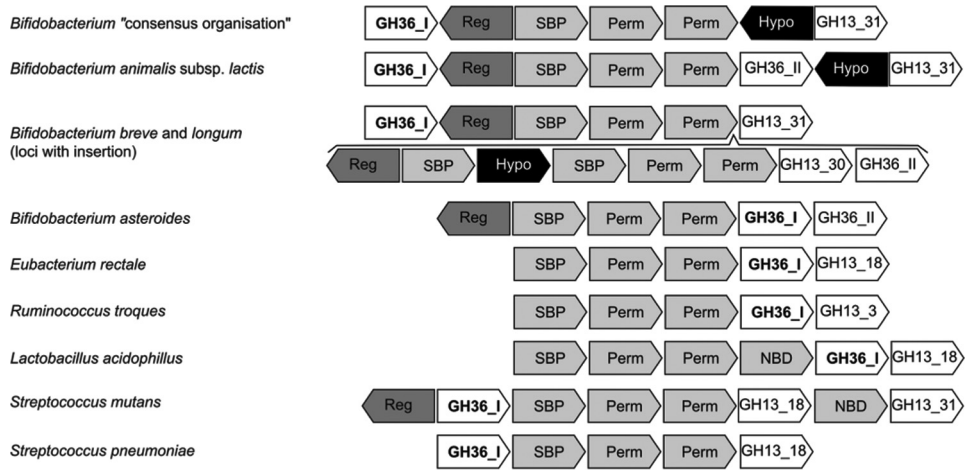

FIGURE 5. **Representative organization of α-(1,6)-galactoside/glucoside utilization loci in bifidobacteria and other HGM taxa in addition to *Streptococcus* strains that colonize the oral cavity and lungs in humans.** The loci are aligned with respect to the ABC transport system (*light gray*) and consisting of SBP and two adjacent transmembrane domain permease genes (*Perm*). Glycoside hydrolases are *white*, and raffinose-specific α-galactosidases of GH36 subfamily 1 (GH36_I) are in *bold*. Transcriptional regulators are *dark gray*, and hypothetical genes are *black*. The consensus organization found in most bifidobacteria is shown on *top* followed by the organization found in *B. animalis* subsp. *lactis*. Distinct *B. longum* and *B. breve* strains have a longer insertion in the locus.

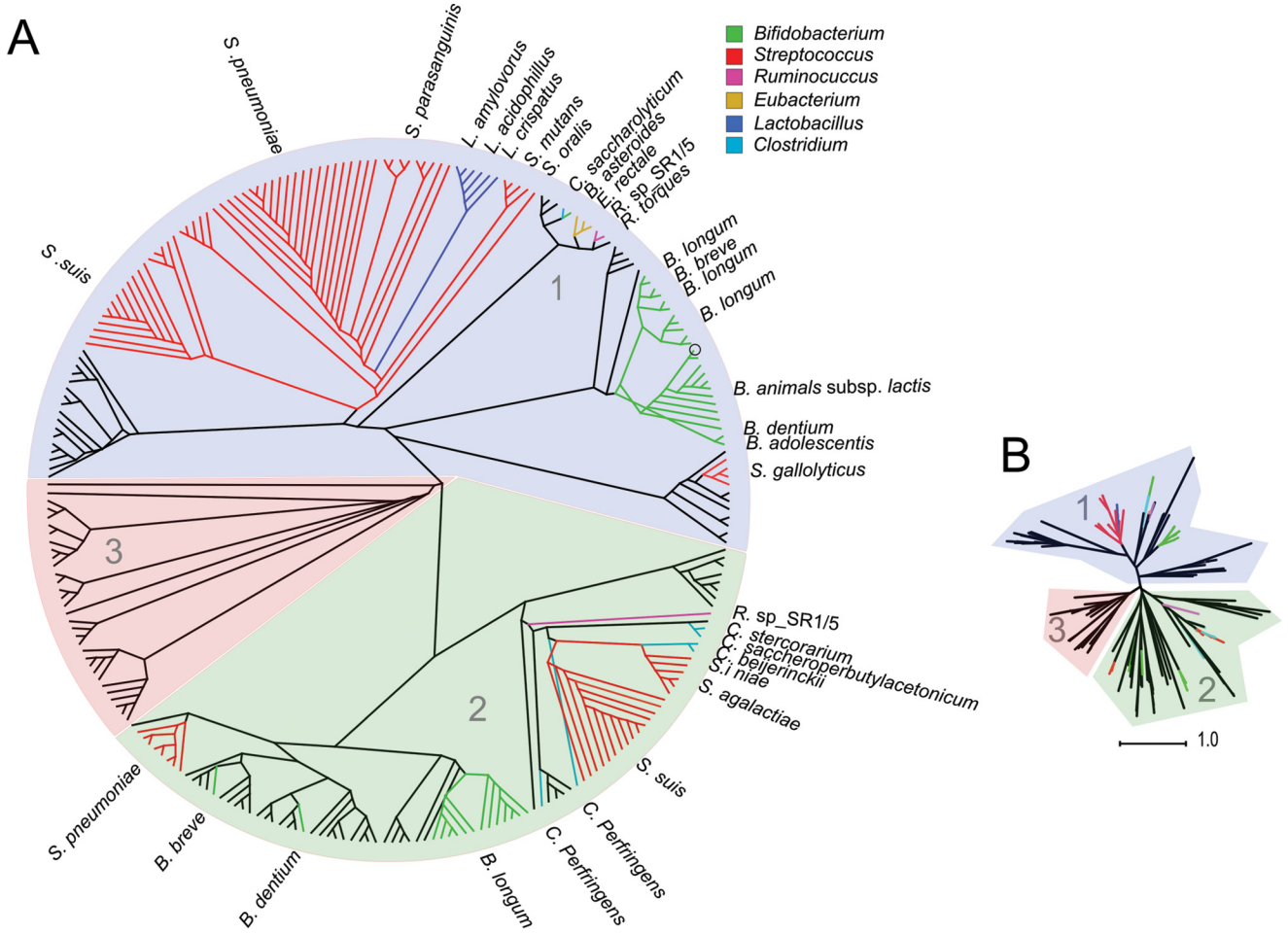

FIGURE 6. **Phylogenetic tree of *Bl*G16BP homologues.** *A*, radial cladogram of the homologues of *Bl*G16BP, which were identified based on the co-localization of their genes with those encoding GH36 enzymes. The cladogram is divided into three subtrees: subtree 1 (*blue background*), subgroup 2 (*green background*), subtrees 3 (*red background*). Subtree 1 contains α-(1,6)-galactoside/glucoside-specific sequences including *Bl*G16BP and functionally related homologues from *Streptococcus* in addition to *Lactobacillus* sequences specific for raffinose family α-(1,6)-galactosides. In agreement with this functional assignment, genes encoding sequences in subtree 1 are co-localized with genes of α-galactosidases (GH36_I) targeting raffinose family α-(1,6)-galactosides. Most sequences belonging to subtree 2 are distinguished by co-localization of their genes with putative α-*N*-acetylgalactosaminidase genes, which suggests a functional role in metabolism of host *O*-glycans. The specificities of subtree 3 SBPs are unknown. The branches from subtree 1 are populated by sequences from genera adapted to the human lung, oral cavity, and gut ecological niches. *B*, phylogram representation of the tree to show pylogentic distances.

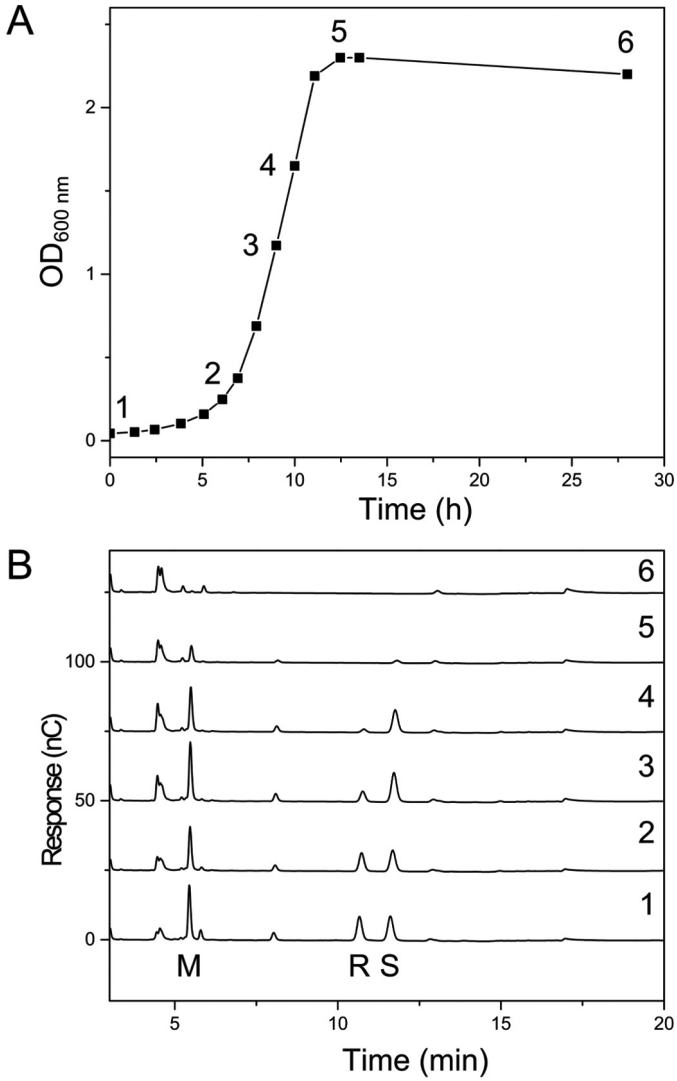

FIGURE 7. **Uptake of raffinose family α-(1,6)-galactosides by *B. animalis* subsp. *lactis* Bl-04.** *A*, growth curve of *B. animalis* subsp. *lactis* Bl-04 supplemented with a 0.5% (w/v) mixture of melibiose, raffinose, and stachyose in equal amounts. The numbers indicate sampling time points for oligosaccharide analysis of culture supernatants. *B*, high performance anion exchange chromatography with per amperometric detection analysis of the fermentation supernatants with the same numbering as in *panel A*. The peaks corresponding to melibiose (*M*), raffinose (*R*), and stachyose (*S*) are indicated.

throughout the growth experiment. Raffinose was depleted first followed by stachyose and, thereafter, melibiose (Fig. 7).

Growth of Bifidobacteria and B. ovatus on α-(1,6)-Glycosides—Growth of seven strains of bifidobacteria on raffinose or a mixture of IMOs was performed. All tested strains except *Bifidobacterium bifidum*, which lacks the genes encoding the *Bl*G16BP ABC transporter, grew efficiently on both raffinose and the IMO mixture (Table 4). Moreover, *B. ovatus* from the dominant human commensal Bacteroidetes phylum, was able to grow equally well on these substrates (Table 4). This shows that growth on α-(1,6)-glycosides does not require ABC-mediated transport as *Bacteroides* lack this type of transporters.

Competition Assay between B. ovatus and B. animalis subsp. lactis Bl-04—We wanted to evaluate the ability of *B. ovatus* to compete with *B. animalis lactis* Bl-04 for raffinose, the preferred substrate for the *Bl*G16BP ABC transporter. *B. animalis lactis* Bl-04 efficiently out-competed *B. ovatus* and accounted for ~98% of the colony-forming units after 18 h of growth in cultures starting from a 50:50 mixture. This distribution persisted after a second round of co-culture (Fig. 8).

TABLE 4
Growth of different bifidobacteria and *B. ovatus* on raffinose and a mixture of isomaltooligosaccharides
Growth was reported as final A_{600} on 0.5% (w/v) carbohydrate. ND, not determined.

Strains	Raffinose	IMO mix
B. animalis subsp. *lactis* Bl-04	1.8 ± 0.05	2.0 ± 0.16
B. adolescentis ATCC 15703	2.4 ± 0.05	2.7 ± 0.05
B. longum subsp. *longum* JCM 1217	1.7 ± 0.01	1.4 ± 0.05
B. longum subsp. *infantis* ATCC 15697	0.8 ± 0.12	2.0 ± 0.15
B. breve ATCC 15648	1.5 ± 0.31	1.6 ± 0.17
B. dentium Bd1	1.1 ± 0.10	1.2 ± 0.08
B. bifidum ATCC 29521	ND	ND
B. ovatus ATCC 8483	1.9 ± 0.01	1.8 ± 0.13

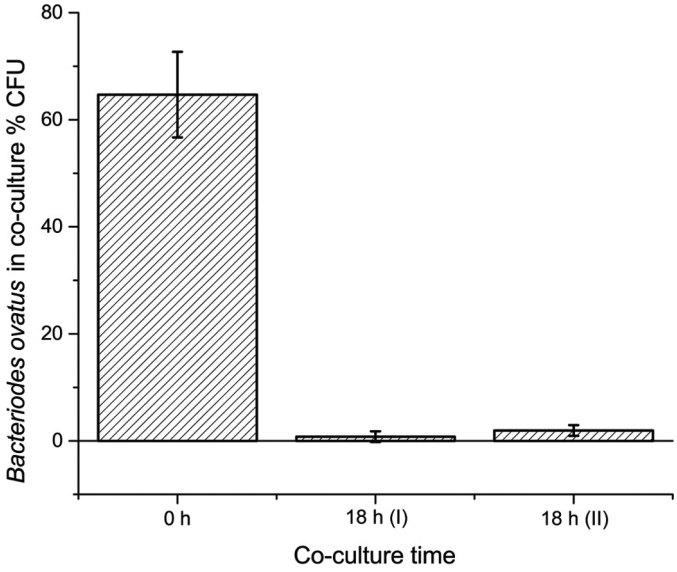

FIGURE 8. **Competition co-cultures between *B. ovatus* and *B. animalis* subsp. *lactis* Bl-04.** *B. animalis* subsp. *lactis* Bl-04 and *B. ovatus* were co-cultured on 0.5% (w/v) raffinose, and the proportion of *B. ovatus* as compared with the total colony forming units in the co-cultures was determined by plating on selective media and viable counts.

Discussion

The complexity and the density of the HGM are highest in the distal gut, reaching 10^{11} cells g^{-1} content (30). Humans consume large amounts of non-digestible glycans that reach the colon intact and exert a significant effect on the composition of the microbiota (9). Uptake of glycan oligomers is likely to be a key adaptation strategy to the fierce competition as it allows further intracellular (or periplasmic) breakdown of these oligomers and precludes loss to competing taxa. The involvement of ABC transporters in uptake of non-digestible oligosaccharides in health-stimulating bacteria has been highlighted through several "omics" studies (22, 31–33), and elevated levels of acetate derived from carbohydrate fermentation and the occurrence of certain carbohydrate specific ABC transporters in *Bifidobacterium* have been correlated to protection against pathogens in a mouse model (34). In this study, we report the structural and biochemical properties of the SBP associated to a conserved bifidobacterial ABC transport system, which has been shown to be transcriptionally up-regulated in response to

growth on a variety of α-glucosides and α-galactosides sharing a common α-(1,6)-disaccharide motif in *B. animalis* subsp. *lactis* (22).

*Basis of Specificity and Size Selection by BlG16BP—Bl*G16BP accommodates α-(1,6)-glycosides varying in size, glycosidic linkage, and monosaccharide composition. A key structural feature that contributes to this plasticity is the recognition of either an equatorial (glucosyl) or an axial (galactosyl) C4-OH at the non-reducing glycosyl unit (position 1) (Fig. 4). Occupancy of this position and an α-(1,6)-glycosidic bond to a glucosyl moiety at position 2 seem to be prerequisites for efficient ligand binding, as judged by the lack of detectable affinity for sucrose (α-d-Glc*p*-(α1,β2)-d-Fru*f*), isomaltulose (α-d-Glc*p*-α-(1–6)-d-Fru*f*), or maltose (α-d-Glc*p*-α-(1–4)-d-Glc*p*). A second feature that contributes to the broad recognition is the lack of direct polar contacts with the glycosyl moiety bound at position 3, which together with the open architecture of the binding site allows the accommodation of either a fructosyl or a glucosyl residue at this position (Fig. 4). Rearrangement of solvent-mediated hydrogen bonds at position 3 seems to allow fine-tuning of ligand contacts as observed in other SBP (25). This is likely to contribute to the large observed entropic penalty of binding and is consistent with an enthalpy-driven binding process (35). The fast kinetics, observed in the SPR analysis are also consistent with the solvent-accessible open binding site architecture (36) and the relatively low density of protein-ligand polar contacts. By contrast, the capture of arabinoxylo-oligosaccharides in a solvent-occluded binding site in another SBP homologue from the same organism was associated with significantly slower binding and dissociation kinetics (25).

Finally, the open binding cleft of *Bl*G16BP allows the extension of the size of the ligands beyond a trisaccharide. Growth of *B. animalis* subsp. *lactis* Bl-04 on the tetrasaccharide (stachyose) and pentasaccharide (verbascose) has been demonstrated (37), which proves that these ligands are indeed taken up albeit with lower selectivity than raffinose the preferred ligand. The preference for trisaccharides was also confirmed by monitoring the depletion of melibiose, raffinose, and stachyose during growth of *B. animalis* subsp. *lactis* Bl-04 (Fig. 7). The order of depletion of these ligands was identical to their measured relative affinities to *Bl*G16BP. This supports the role of the *Bl*G16BP ABC system in the uptake of these α-(1,6)-galactosides.

Comparison of BlG16BP to the Distantly Related RafE from S. pneumoniae—The structure of the *Bl*G16BP homologue RafE, from *S. pneumoniae* in complex with raffinose, has been deposited (PDB code 2i58). Despite low levels of sequence conservation, *Bl*G16BP and RafE share fold and domain organization (Fig. 4). Differences between these two proteins are observed in the ligand aromatic stacking platform, which in RafE comprises three tryptophans and a tyrosine residue. Two of these tryptophans are substituted by the less bulky Tyr-291 and Phe-392 at positions 1 and 2, respectively, in *Bl*G16BP (Fig. 4). The role of the RafE-associated ABC transport system in uptake of melibiose, raffinose, and isomaltotriose has been demonstrated by gene knock-out (38) and transcriptional analyses (39). Gene knockouts in *Bifidobacterium* are not straight forward to introduce, but the functional and structural similarity between *Bl*G16BP and RafE supports the role of *Bl*G16BP ABC systems in the uptake of α-(1,6)-glycosides in *Bifidobacterium*. This is further supported by uptake profile analysis in *B. animalis* subsp. *lactis* Bl-04 and the inability of the only tested *Bifidobacterium* strain, which lacks this ABC system, to grow on α-(1,6)-glycosides (Table 4).

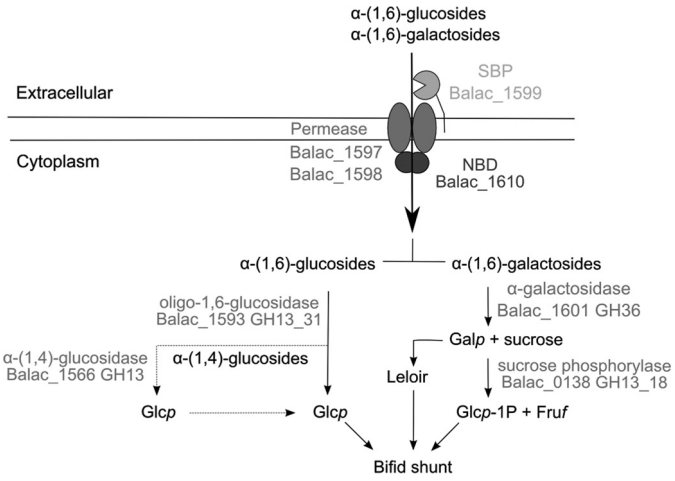

FIGURE 9. **Uptake and metabolism model of α-(1,6)-galactoside/glucoside by *B. animalis* subsp. *lactis* and the other bifidobacteria possessing a similar system (see Fig. 6).** *Bl*G16BP (Balac_1599), which is anchored to the extracellular side of the cell membrane by a lipid anchor, captures α-(1,6)-galacto-oligosaccharides (*RFO*) and α-(1,6)-gluco-oligosaccharides (*IMO*), which are translocated to the cytoplasm by the ABC transport system (Balac_1598, Balac_1597, and Balac_1610). The α-galactosidase (Balac_1601) and the α-(1,6)-glucosidase are responsible for the degradation of α-(1,6)-galactosides and α-(1,6)-glucosides, respectively, based on transcriptional data (22) and homology to characterized counterparts. α-(1,4)-Glucosidases and sucrose phosphorylases are possible candidates for the degradation of the maltose moiety of panose and the sucrose moiety of raffinose, respectively, into glucose and galactose, which is converted into glucose 1-phosphate via the Lelior pathway before entering the bifid shunt. *Leloir* refers to the Leloir pathway a metabolic pathway for catabolism of galactose.

α-(1,6)-Glycoside Metabolism in the Human Gut Niche and Possible Advantages of ABC-mediated Transport—Our genetic and phylogenetic analyses assert the conservation of the *Bl*G16BP ABC system in most human gut-adapted bifidobacteria together with the necessary machinery for breakdown of α-(1,6)-linked galactosides and glucosides, which outlines the utilization route of these glycans (Figs. 6 and 9). This is in accord with the high activity of the oligo α-(1,6)-glucosidase encoded by this locus in *Bifidobacterium adolescentis* toward isomaltose and isomaltotriose (40). The co-occurrence of α-(1,6)-galactosides and glucosides in plant seeds, *e.g.* soybean (41), provides a possible explanation for the catabolic integration of the above two classes of glycans in both bifidobacteria and streptococci. Notably, this clustering is not observed in *Eubacterium*, *Ruminococcus*, and *Lactobacillus* HGM strains, which lack the α-(1,6)-glucosidase gene (Fig. 5). Thus, only α-(1,6)-galactosides are likely to be taken up by the ABC system in theses Firmicutes taxa, which are supported by transcriptional analysis in *L. acidophilus* NCFM (32). Interestingly, this α-(1,6)-galactoside specific ABC system is only present in acidophilus cluster human gut-adapted lactobacilli (28). The lack of this ABC system in *Lactobacillus* strains from other ecological niches suggests recent acquisition of this transporter by horizontal gene transfer during the adaptation to the human

gut. Acquisition of oligosaccharide uptake and catabolism genes has been proposed as an adaptation strategy to the gut niche (42). With the exception of *Bifidobacterium* and a few strains from Firmicutes, the *Bl*G16BP ABC system seems to be lacking in most HGM commensals, including those able to degrade α-(1,6)-glycosides, but use different transporters, *e.g.* the major facilitator superfamily melibiose uptake system present in some *E. coli* strains (43). We have shown in the present study that *B. ovatus*, which uses SusC-type glycan transporters, was able to efficiently grow on raffinose the preferred RFO ligand for the *Bl*G16BP ABC system in monocultures. *B. animalis* subsp. *lactis* Bl-04, however, was able to efficiently outcompete *B. ovatus* in mixed cultures. These findings suggest that the preferential stimulation of bifidoabcteria by raffinose is most likely attributed to the competitive advantage granted by ABC-mediated transport in the uptake of short α-1,6-oligosaccharides (Fig. 8).

The affinity range of ligand binding to *Bl*G16BP is roughly 2 orders of magnitude lower than the only two previously characterized oligosaccharide binding proteins from bifidobacteria (25, 44). The lower affinity may reflect the level of competition for the preferred ligands of the transporter in the gut. This is in agreement with the relatively narrow taxonomic distribution of ABC-mediated uptake of α-(1,6)-glycosides in the gut system revealed by our analyses. Obviously this μM affinity is still much higher than the reported 1 mM affinity estimated for the melibiose symporter from *E. coli* (43). The fact that *B. animalis* subsp. *lactis* virtually was able to out-compete *Bacteroides* suggests that the affinities of SusC systems of *Bacteroides* are much lower for raffinose than the *Bl*G16BP ABC system.

In conclusion, this study reports the first biochemical and structural insight into an ABC-associated α-(1,6)-glycoside transport protein and provides evidence that ABC-mediated uptake may confer a competitive edge in the fierce competition for metabolic resources in the human gut niche. Altogether, these findings promote our understanding of the impact of oligosaccharide uptake in preferential glycan utilization.

Experimental Procedures

Cloning, Production, and Purification of the Solute Binding Protein Balac_1599 from B. animalis subsp. lactis Bl-04—*B. animalis* subsp. *lactis* Bl-04 genomic DNA was used as the template for the PCR amplification of the Balac_1599 open reading frame (GI:241191602) with the primers sense (5′-GAATTC**CATATG**GGCAGCGGGCAGGTCACGCTC-3′) and antisense (5′-CGC**GGATCC**CTACTTGCGGAAGTCACGAGCC-3′). The PCR amplicon (1201 base pairs) encoding the mature peptide without the signal peptide as predicted by SignalP (SignalP 4.1 Server) was cloned within the NdeI and BamHI restriction sites (in bold) of pET28a(+) (Novagen, Darmstadt, Germany) and transformed into *E. coli* DH5α (Invitrogen). The resulting pET28aBalac1599 was fully sequenced and transformed into *E. coli* BL21(DE3) and B834DE3 (Novagen) for expression of unlabeled and selenomethionine-labeled protein, respectively.

Recombinant Balac_1599, designated *Bl*G16BP (α-(1,6)-glycoside binding protein from *B. lactis*) was produced as an N-terminal fusion with a hexahistidine purification tag in a 5-liter Biostat B bioreactor (B. Braun Biotech International, Melsungen, Germany) as previously described (45) with the following modifications; heterologous expression was induced at 37 °C, and the cells were harvested after 5 h by centrifugation (10,000 × *g* at 4 °C for 15 min) and stored at −20 °C. Selenomethionine-labeled *Bl*G16BP was produced in B834DE3 according to Studts and Fox (46).

The recombinant protein was purified by immobilized metal ion affinity chromatography using a 5-ml HisTrap HP column (GE Healthcare) as described (45) followed by anion exchange chromatography using an 8-ml Mono Q 10/100 GL column (GE Healthcare) equilibrated in 20 mM sodium phosphate, pH 7.0 (buffer A), and installed on an ÄKTA Avant chromatograph (GE Healthcare). Proteins eluted by a gradient of buffer B (buffer A + 500 mM NaCl) in 10 column volumes at 1 ml min^{-1} were analyzed by SDS-PAGE, pure fractions were pooled, and buffer was exchanged into 20 mM sodium phosphate, pH 7.0. The N-terminal tag was removed by incubation with thrombin from Novagen for 24 h at room temperature and passed through the His column, the flow-through containing the cleaved recombinant protein was concentrated, and buffer was exchanged into 20 mM phosphate, pH 7.0. Protein concentration was determined by measuring, A_{280} using a molar extinction coefficient $\epsilon_{280\,nm} = 51{,}750\ M^{-1}cm^{-1}$ determined experimentally by amino acid analysis (predicted $\epsilon_{280\,nm} = 45{,}380\ M^{-1}cm^{-1}$).

Carbohydrates—Fructose, galactose, glucose, melibiose, sucrose, malto-oligosaccharides DP (degree of polymerization) 2–7 ([α-d-Glc*p*-(1–4)]$_{n=1-6}$-d-Glc*p*), isomaltulose (α-d-Glc*p*-α-(1–6)-d-Fru*f*), raffinose (α-d-Gal*p*-(1–6)-α-d-Glc*p*-(1–2)-β-d-Fru*f*), stachyose (α-d-Gal*p*-(1–6)-α-d-Gal*p*-(1–6)-α-d-Glc*p*-(1–2)-β-d-Fru*f*), and verbascose (α-d-Gal*p*-(1–6)-α-d-Gal*p*-(1–6)-α-d-Gal*p*-(1–6)-α-d-Glc*p*-(1–2)-β-d-Fru*f*) were from Sigma. β-1,4-Xylo-oligosaccharides ([β-d-xyl*p*-(1,4)]$_{n=1-6}$-d-xyl*p*) were from Shandong Longlive Biotechnology Co., Ltd. (Yucheng, China). Cellobiose (β-d-Glc*p*-(1,4)-d-Glc*p* was from Fluka AG (St. Gallen, Switzerland). β-Galacto-oligosaccharides (both [β-d-Gal*p*-(1,4)]$_{n=1-5}$-d-Glc*p* and [β-d-Gal*p*-(1,6)]$_{n=1-5}$-d-Glc*p*) and fructo-oligosaccharides ([β-d-Fru*f*-(1–2)]$_{n=1-5}$-(β2,α1)-d-Glc*p*) were kindly supplied from DuPont Health and Nutrition Inc. (Brabrand, Denmark) as custom preparations. Panose and isomaltotriose were from Carbosynth (Berkshire, UK), whereas IMOs FP (degree of polymerization) 4–7 were a kind gift of Prof. Atsuo Kimura (Hokkaido University, Hokkaido, Japan) (See Fig. 1). For the growth experiments, a commercial mixture of IMO was used (Wako Pure Chemical Industries, Osaka, Japan), and the α-mannan was from Orffa (Werkendam, The Netherlands).

Surface Plasmon Resonance (SPR)—The SPR analysis was performed using a Biacore T100 (GE Healthcare). *Bl*G16BP (100 μg/ml) diluted in 10 mM sodium acetate, pH 4.5, was immobilized onto a CM5 chip (GE Healthcare) using a standard amine coupling protocol to a density of 3900 response units. Binding analyses were carried out at 25 °C in 20 mM phosphate, pH 7.0, 150 mM sodium chloride, 0.005% (v/v) P20 (GE Healthcare) running buffer unless otherwise stated, and all solutions were filtered before analysis (0.22 μm). In the initial screening of binding, 1 mM carbohydrate in running buffer was injected

over the chip surface at 30 μl min^{-1} with association and dissociation times of 90 and 180 s, respectively. Affinities of carbohydrates showing binding to the immobilized *Bl*G16BP were measured using at least 10 concentrations in the ranges 3.9–1000 μM IMO, 3–1600 μM melibiose, 0.24–1000 μM raffinose, and 8–4000 μM stachyose or verbascose. The pH dependence was measured using four concentrations of raffinose (4–250 μM) in 20 mM sodium acetate, pH 4.0–5.5, 20 mM sodium citrate-phosphate, pH 5.5–8.0, and a similar NaCl and surfactant concentration as in the running buffer. Dissociation constants (K_D) were determined by fitting a one-binding site model to the steady state sensograms. No binding was measured of cellobiose, β-1,4-xylo-oligosaccharides, β-galacto-oligosaccharides, β-fructo-oligosaccharides, or α-1,4-gluco-oligosaccharides (malto-oligosaccharides).

ITC—The affinity of *Bl*G16BP to the preferred ligands raffinose and panose was determined by ITC (ITC_{200}; GE Healthcare). Titrations were conducted in triplicate at 25 °C by injection of 2 mM raffinose or panose into 108 μM *Bl*G16BP in 20 mM sodium citrate-phosphate, pH 7.0. Injection of panose and raffinose into buffer was performed for measuring the heat of dilution, which was subtracted in the data analysis. The ITC experiments included a preinjection of 0.5 μl, which was discarded from the analysis followed by 38 × 1-μl injections into an ITC cell volume of 204 μl. The ITC heat traces were processed as described previously (47), and a one-site binding model governed by the equilibrium association constant, K_A, the molar enthalpy for binding, ΔH, and the average number of binding sites on the protein, n, were included as fitting parameters.

Crystallization and Structure Determination—Crystals were only obtained in the presence of either panose or raffinose (1 mM) by vapor diffusion in hanging or sitting drops and grew for 60 h at 5 °C at a 1:1 ratio of *Bl*G16BP and reservoir solution. An initial crystallization condition (0.1 M Tris, pH 8.5, 30% PEG-4000, and 0.2 M $MgCl_2$ at 278 K) was identified with the Structure Screen (Molecular Dimensions Ltd, UK) using a Mosquito® liquid handling robot (TTP Labtech). Crystal growth of *Bl*G16BP and selenomethionine-labeled *Bl*G16BP (15 mg·ml^{-1} in 10 mM MES, pH 6.5, and 150 mM NaCl) was optimized in reservoir solution of 0.1 M Tris, pH 8.5, 25% PEG 4000, 0.8 M $MgCl_2$ and 0.1 M Tris, pH 8.5, 21% PEG 4000, and 1.0 M $MgCl_2$ for the selenomethionine *Bl*G16BP. Due to the high concentrations of PEG in the reservoir solution, no further cryo-protectant was needed, and the crystals were flash-frozen directly in liquid nitrogen. Diffraction data were collected to a maximum resolution of 2.1 Å for selenomethionine-labeled *Bl*G16BP:raffinose, 1.4 Å for *Bl*G16BP:raffinose, 1.8 Å for *Bl*G16BP:panose at SLS beamlines PXI and PXIII, Villigen, Switzerland and MAX-lab, Lund, Sweden. All datasets were processed with XDS (48). The structure of selenomethionine *Bl*G16BP was solved in the orthorhombic space group $P2_12_12_1$ using the single-wavelength anomalous diffraction (SAD) method with the experimental phase information obtained from data collected at the Selenium K-edge. The program Phenix.AutoSol (49, 50) identified all nine selenium atoms from nine possible selenomethionyl residues present in the *Bl*G16BP. An initial partial model was obtained with Phenix.AutoBuild (51), and further corrections and model building using the program Coot (52) resulted in a complete model, which was used in molecular replacement to solve the structure of *Bl*G16BP:raffinose. The models were refined using phenix.refine (53) randomly setting aside 5% of the reflections. Molecular replacement with the protein part of *Bl*G16BP:raffinose was used to solve the *Bl*G16BP-panose complex. Ligand molecules were included after the protein atoms were built, and water molecules were added with Coot manually. The overall quality of all models was checked using MolProbity (49). The final models of *Bl*G16BP in complex with raffinose and panose were refined to R_{cryst}/R_{free} values of 0.13/0.17 and 0.16/0.21, respectively. The models are deposited in the Protein Data Bank (PDB) with accession codes 4ZS9, 4ZZE, and 4ZZA for the raffinose, panose, and selenomethionine-labeled raffinose complex, respectively. The two complexes are very similar in conformation, and superposition of the individual models results in pairwise overall r.m.s.d. of 0.4 Å between aligned C_α atoms. The PyMOL Molecular Graphics System, Version 1.7.2.2 Schrödinger, LLC was used to explore the models and for rendering.

Phylogenetic and Genetic Analysis of SBPs Potentially Conferring the Uptake of α-(1,6) Glycosides—An analysis of bifidobacterial close orthologues of *Bl*G16BP was performed by a blast search against refseq database within *Bifidobacterium* with an a sequence identity of >50% were selected. The resulting 40 protein sequences were aligned using MAFFT (54); this alignment was used to calculate the degree of conservation for each residue. The organization of genes flanking the putative RFO/IMO binding proteins was visualized using the Microbial Genomic context Viewer server (MGcV) (55). The genes flanking putative RFO/IMO-binding proteins within a genetic context range of 40,000 base pairs (bp) were analyzed manually to assess the presence of permease component genes of ABC transporters and relevant glycoside hydrolases featuring in RFO or IMO catabolism. These criteria were applied to define bifidobacterial RFO/IMO utilization loci. To investigate the occurrence of *Bl*G16BP orthologues in a wider taxonomic range, all GH36 α-galactosidase sequences of bacterial origin were extracted from the CAZy database (56). The resulting 1050 sequences were submitted to the MGcV server, and all solute-binding protein-encoding genes located within 20,000 bp of a GH36 α-glactosidase encoding gene were selected. The resulting 263 sequences were aligned using MAFFT, and a phylogenetic tree was computed.

Growth of Anaerobic Bacteria and Competition Assays—Monocultures of *B. animalis* subsp. *lactis* Bl-04, *B. adolescentis* ATCC 15703, *B. longum* subsp. *longum* JCM 1217, *B. longum* subsp. *infantis* ATCC 15697, *Bifidobacterium breve* ATCC 15648, *Bifidobacterium dentium* Bd1, *B. bifidum* ATCC 29521, and *B. ovatus* ATCC 8483 were grown anaerobically in LAB SEM medium (1% bactopeptone (wt/vol) (Lab M), 0.5% yeast extract (wt/vol) (Lab M), 0.2% dipotassium phosphate (wt/vol) (Sigma), 0.5% sodium acetate (wt/vol) (Merck), 0.2% ammonium citrate (wt/vol) (Sigma), 0.02% magnesium sulfate (wt/vol) (Sigma), 0.005% manganese sulfate (wt/vol) (Sigma), 0.1% Tween 80 (vol/vol) (Sigma), and 0.5% carbohydrate (wt/vol)) (33) containing 0.5% (w/v) of either raffinose or a commercial mixture of isomalto-oligosaccharides at 37 °C for 18 h, and the final A_{600} was measured.

To evaluate the competition between *B. animalis* subsp. *lactis* Bl-04 and *B. ovatus* ATCC 8483, the strains were grown as above in the presence of 0.5% (w/v) raffinose. Equal A_{600} units of both strains were used to inoculate a co-culture to $A_{600} \approx 0.1$ in the same medium. The co-culture was incubated at 37 °C anaerobically for 18 h and subsequently used to inoculate a second co-culture in the same medium, after which growth was continued for 18 h. To compare the ratios of *B. animalis* subsp. *lactis* Bl-04 and *B. ovatus*, serial dilutions of both co-cultures were plated on BHI-agar plates supplemented with 0.5% (w/v) raffinose (both strains grow on these plates) and LAB SEM-agar supplemented with 0.5% (w/v) α-mannan (only *B. ovatus* grows on this substrate) to obtain single colonies. The ratio of colony forming units (cfu) on the *Bacteroides*-selective plate was compared with the total cfu from the plate sustaining the growth of both strains.

Analysis of Oligosaccharide Uptake Profile—B. animalis subsp. *lactis* Bl-04 was grown in LAB SEM medium supplemented with 0.5% (w/v) of an equal mixture of melibiose, raffinose, and stachyose. Aliquots were withdrawn from the cultures at six time intervals, and oligosaccharides in culture supernatants were analyzed by high performance anion-exchange chromatography with pulsed amperometric detection (HPAEC-PAD) (Dionex) using a Carbopac PA200 column and a mobile phase (0.35 ml/min) of constant 100 mM NaOH and a gradient of sodium acetate 0-20 min of 0-160 mM and 20-25 min of 160-400 mM with 10-μl sample injections. Standards (50 μM) of melibiose, raffinose, and stachyose were used to identify the peaks in the chromatograms. Samples were diluted in 200-fold in Milli-Q water and subsequently 10-fold in 100 mM NaOH before analysis and compared with the standards.

Author Contributions—J. M. A., M. E., F. F., B. S., D. J. S., and M. A. H. planned the experiments, interpreted the data, and wrote the paper. J. M. A. and M. E. designed and analyzed the experiments in Fig. 2 and Table 1. J. M. A., J. R. H., and T. L. A. designed and analyzed the experiments in Fig. 3 and Table 2. M. E., A. V. Z., and F. F. designed and analyzed the experiments in Fig. 3 and Table 2. All authors reviewed the results and approved the final version of the manuscript.

Acknowledgment—We thank Alexander Holm Viborg for the development of the CAZy tools, which were used in the phylogenetic analysis.

References

1. Eckburg, P. B., Bik, E. M., Bernstein, C. N., Purdom, E., Dethlefsen, L., Sargent, M., Gill, S. R., Nelson, K. E., and Relman, D. A. (2005) Diversity of the human intestinal microbial flora. *Science* **308,** 1635–1638
2. Ley, R. E., Hamady, M., Lozupone, C., Turnbaugh, P. J., Ramey, R. R., Bircher, J. S., Schlegel, M. L., Tucker, T. A., Schrenzel, M. D., Knight, R., and Gordon, J. I. (2008) Evolution of mammals and their gut microbes. *Science* **320,** 1647–1651
3. Sommer, F., and Bäckhed, F. (2013) The gut microbiota: masters of host development and physiology. *Nat. Rev. Microbiol.* **11,** 227–238
4. Cryan, J. F., and Dinan, T. G. (2012) Mind-altering microorganisms: the impact of the gut microbiota on brain and behaviour. *Nat. Rev. Neurosci.* **13,** 701–712
5. Nicholson, J. K., Holmes, E., Kinross, J., Burcelin, R., Gibson, G., Jia, W., and Pettersson, S. (2012) Host-gut microbiota metabolic interactions. *Science* **336,** 1262–1267
6. Brown, K., DeCoffe, D., Molcan, E., and Gibson, D. L. (2012) Diet-induced dysbiosis of the intestinal microbiota and the effects on immunity and disease. *Nutrients* **4,** 1095–1119
7. David, L. A., Maurice, C. F., Carmody, R. N., Gootenberg, D. B., Button, J. E., Wolfe, B. E., Ling, A. V., Devlin, A. S., Varma, Y., Fischbach, M. A., Biddinger, S. B., Dutton, R. J., and Turnbaugh, P. J. (2014) Diet rapidly and reproducibly alters the human gut microbiome. *Nature* **505,** 559–563
8. Muegge, B. D., Kuczynski, J., Knights, D., Clemente, J. C., González, A., Fontana, L., Henrissat, B., Knight, R., and Gordon, J. I. (2011) Diet drives convergence in gut microbiome functions across mammalian phylogeny and within humans. *Science* **332,** 970–974
9. Koropatkin, N. M., Cameron, E. A., and Martens, E. C. (2012) How glycan metabolism shapes the human gut microbiota. *Nat. Rev. Microbiol.* **10,** 323–335
10. Mäkeläinen, H., Hasselwander, O., Rautonen, N., and Ouwehand, A. C. (2009) Panose, a new prebiotic candidate. *Lett. Appl. Microbiol.* **49,** 666–672
11. Andersen, K. E., Bjergegaard, C., Møller, P., Sørensen, J. C., and Sørensen, H. (2005) Compositional variations for α-galactosides in different species of Leguminosae, Brassicaceae, and barley: a chemotaxonomic study based on chemometrics and high-performance capillary electrophoresis. *J. Agric. Food Chem.* **53,** 5809–5817
12. Jukanti, A. K., Gaur, P. M., Gowda, C. L., and Chibbar, R. N. (2012) Nutritional quality and health benefits of chickpea (Cicer arietinum L.): a review. *Br. J. Nutr.* **108,** S11–S26
13. Ao, Z., Simsek, S., Zhang, G., Venkatachalam, M., Reuhs, B. L., and Hamaker, B. R. (2007) Starch with a slow digestion property produced by altering its chain length, branch density, and crystalline structure. *J. Agric. Food Chem.* **55,** 4540–4547
14. Swennen, K., Courtin, C. M., and Delcour, J. A. (2006) Non-digestible oligosaccharides with prebiotic properties. *Crit. Rev. Food Sci. Nutr.* **46,** 459–471
15. Ishizuka, S., Iwama, A., Dinoto, A., Suksomcheep, A., Maeta, K., Kasai, T., Hara, H., and Yokota, A. (2009) Synbiotic promotion of epithelial proliferation by orally ingested encapsulated *Bifidobacterium breve* and raffinose in the small intestine of rats. *Mol. Nutr. Food Res.* **53,** S62–S67
16. Ventura, M., O'Connell-Motherway, M., Leahy, S., Moreno-Munoz, J. A., Fitzgerald, G. F., and van Sinderen, D. (2007) From bacterial genome to functionality; case bifidobacteria. *Int. J. Food Microbiol.* **120,** 2–12
17. Flint, H. J., and Bayer, E. A. (2008) Plant cell wall breakdown by anaerobic microorganisms from the mammalian digestive tract. *Ann. N.Y. Acad. Sci.* **1125,** 280–288
18. Flint, H. J., Duncan, S. H., Scott, K. P., and Louis, P. (2007) Interactions and competition within the microbial community of the human colon: links between diet and health. *Environ. Microbiol.* **9,** 1101–1111
19. Pokusaeva, K., Fitzgerald, G. F., and van Sinderen, D. (2011) Carbohydrate metabolism in Bifidobacteria. *Genes Nutr.* **6,** 285–306
20. ter Beek, J., Guskov, A., and Slotboom, D. J. (2014) Structural diversity of ABC transporters. *J. Gen. Physiol.* **143,** 419–435
21. Berntsson, R. P., Smits, S. H., Schmitt, L., Slotboom, D. J, and Poolman, B. (2010) A structural classification of substrate-binding proteins. *FEBS Lett.* **584,** 2606–2617
22. Andersen, J. M., Barrangou, R., Abou Hachem, M., Lahtinen, S. J., Goh, Y. J., Svensson, B., and Klaenhammer, T. R. (2013) Transcriptional analysis of oligosaccharide utilization by *Bifidobacterium lactis* Bl-04. *BMC Genomics* **14,** 312
23. Oldham, M. L., Chen, S., and Chen, J. (2013) Structural basis for substrate specificity in the *Escherichia coli* maltose transport system. *Proc. Natl. Acad. Sci. U.S.A.* **110,** 18132–18137
24. Holm, L., and Rosenström, P. (2010) Dali server: conservation mapping in 3D. *Nucleic Acids Res.* **38,** W545–W549
25. Ejby, M., Fredslund, F., Vujicic-Zagar, A., Svensson, B., Slotboom, D. J., and Abou Hachem, M. (2013) Structural basis for arabinoxylo-oligosaccharide capture by the probiotic *Bifidobacterium animalis* subsp. *lactis* Bl-04. *Mol. Microbiol.* **90,** 1100–1112
26. Mahowald, M. A., Rey, F. E., Seedorf, H., Turnbaugh, P. J., Fulton, R. S., Wollam, A., Shah, N., Wang, C., Magrini, V., Wilson, R. K., Cantarel, B. L.,

Coutinho, P. M., Henrissat, B., Crock, L. W., Russell, A., Verberkmoes, N. C., Hettich, R. L., and Gordon, J. I. (2009) Characterizing a model human gut microbiota composed of members of its two dominant bacterial phyla. *Proc. Natl. Acad. Sci. U.S.A.* **106,** 5859–5864
27. Wang, L., Christophersen, C. T., Sorich, M. J., Gerber, J. P., Angley, M. T., and Conlon, M. A. (2013) Increased abundance of *Sutterella* spp., and *Ruminococcus torques* in feces of children with autism spectrum disorder. *Mol. Autism* **4,** 42
28. Barrangou, R., Azcarate-Peril, M. A., Duong, T., Conners, S. B., Kelly, R. M., and Klaenhammer, T. R. (2006) Global analysis of carbohydrate utilization by *Lactobacillus acidophilus* using cDNA microarrays. *Proc. Natl. Acad. Sci. U.S.A.* **103,** 3816–3821
29. Loesche, W. J. (1986) Role of *Streptococcus mutans* in human dental decay. *Microbiol. Rev.* **50,** 353–380
30. Kleerebezem, M., and Vaughan, E. E. (2009) Probiotic and gut lactobacilli and bifidobacteria: molecular approaches to study diversity and activity. *Annu. Rev. Microbiol.* **63,** 269–290
31. Gilad, O., Jacobsen, S., Stuer-Lauridsen, B., Pedersen, M. B., Garrigues, C., and Svensson, B. (2010) Combined transcriptome and proteome analysis of *Bifidobacterium animalis* subsp. *lactis* BB-12 grown on xylo-oligosaccharides and a model of their utilization. *Appl. Environ. Microbiol.* **76,** 7285–7291
32. Andersen, J. M., Barrangou, R., Abou Hachem, M., Lahtinen, S. J., and Goh, Y. J., Svensson, B., Klaenhammer, T. R. (2012) Transcriptional analysis of prebiotic uptake and catabolism by *Lactobacillus acidophilus* NCFM. *PloS ONE* **7,** e44409
33. Barrangou, R., Altermann, E., Hutkins, R., Cano, R., and Klaenhammer, T. R. (2003) Functional and comparative genomic analyses of an operon involved in fructooligosaccharide utilization by *Lactobacillus acidophilus*. *Proc. Natl. Acad. Sci. U.S.A.* **100,** 8957–8962
34. Fukuda, S., Toh, H., Hase, K., Oshima, K., Nakanishi, Y., Yoshimura, K., Tobe, T., Clarke, J. M., Topping, D. L., Suzuki, T., Taylor, T. D., Itoh, K., Kikuchi, J., Morita, H., Hattori, M., and Ohno, H. (2011) Bifidobacteria can protect from enteropathogenic infection through production of acetate. *Nature* **469,** 543–547
35. Jelesarov, I., and Bosshard, H. R. (1999) Isothermal titration calorimetry and differential scanning calorimetry as complementary tools to investigate the energetics of biomolecular recognition. *J. Mol. Recognit.* **12,** 3–18
36. Morton, T. A., and Myszka, D. G. (1998) Kinetic analysis of macromolecular interactions using surface plasmon resonance biosensors. *Methods Enzymol.* **295,** 268–294
37. van Zanten, G. C., Knudsen, A., Röytiö, H., Forssten, S., Lawther, M., Blennow, A., Lahtinen, S. J., Jakobsen, M., Svensson, B., and Jespersen, L. (2012) The effect of selected synbiotics on microbial composition and short-chain fatty acid production in amodel system of the human colon. *PloS ONE* **7,** e47212
38. Russell, R. R., Aduse-Opoku, J., Sutcliffe, I. C., Tao, L., and Ferretti, J. J. (1992) A binding protein-dependent transport-system in *Streptococcus mutans* responsible for multiple sugar metabolism. *J. Biol. Chem.* **267,** 4631–4637
39. Rosenow, C., Maniar, M., and Trias, J. (1999) Regulation of the α-galactosidase activity in *Streptococcus pneumoniae*: characterization of the raffinose utilization system. *Genome Res.* **9,** 1189–1197
40. van den Broek, L. A., Struijs, K., Verdoes, J. C., Beldman, G., and Voragen, A. G. (2003) Cloning and characterization of two α-glucosidases from *Bifidobacterium adolescentis* DSM20083. *Appl. Microbiol. Biotechnol.* **61,** 55–60
41. Goffin, D., Delzenne, N., Blecker, C., Hanon, E., Deroanne, C., and Paquot, M. (2011) Will isomalto-oligosaccharides, a well-established functional food in Asia, break through the European and American market? The status of knowledge on these prebiotics. *Crit. Rev. Food Sci. Nutr.* **51,** 394–409
42. Goh, Y. J., and Klaenhammer, T. R. (2015) Genetic mechanisms of prebiotic oligosaccharide metabolism in probiotic microbes. *Annu. Rev. Food Sci. Technol.* **6,** 137–156
43. Ethayathulla, A. S., Yousef, M. S., Amin, A., Leblanc, G., Kaback, H. R., and Guan, L. (2014) Structure-based mechanism for Na^+/melibiose symport by MelB. *Nat. Commun.* **5,** 3009
44. Suzuki, R., Wada, J., Katayama, T., Fushinobu, S., Wakagi, T., Shoun, H., Sugimoto, H., Tanaka, A., Kumagai, H., Ashida, H., Kitaoka, M., and Yamamoto, K. (2008) Structural and thermodynamic analyses of solute-binding protein from *Bifidobacterium longum* specific for core 1 disaccharide and lacto-*N*-biose I. *J. Biol. Chem.* **283,** 13165–13173
45. Fredslund, F., Abou Hachem, M., Larsen, R. J., Sørensen, P. G., Coutinho, P. M., Lo Leggio, L., and Svensson, B. (2011) Crystal structure of α-galactosidase from *Lactobacillus acidophilus* NCFM: insight into tetramer formation and substrate binding. *J. Mol. Biol.* **412,** 466–480
46. Studts, J. M., and Fox, B. G. (1999) Application of fed-batch fermentation to the preparation of isotopically labeled or selenomethionyl-labeled proteins. *Protein Expr. Purif.* **16,** 109–119
47. Henriksen, J. R., Andresen, T. L., Feldborg, L. N., Duelund, L., and Ipsen, J. H. (2010) Understanding detergent effects on lipid membranes: A model study of lysolipids. *Biophys. J.* **98,** 2199–2205
48. Kabsch, W. (2010) XDS. *Acta Crystallogr. D Biol. Crystallogr.* **66,** 125–132
49. Adams, P. D., Afonine, P. V., Bunkóczi, G., Chen, V. B., Davis, I. W., Echols, N., Headd, J. J., Hung, L.-W., Kapral, G. J., Grosse-Kunstleve, R. W., McCoy, A. J., Moriarty, N. W., Oeffner, R., Read, R. J., Richardson, D. C., Richardson, J. S., Terwilliger, T. C., and Zwart, P. H. (2010) PHENIX: a comprehensive Python-based system for macromolecular structure solution. *Acta Crystallogr. D Biol. Crystallogr.* **66,** *213–221*
50. McCoy, A. J., Grosse-Kunstleve, R. W., Adams, P. D., Winn, M. D., Storoni, L. C., and Read, R. J. (2007) Phaser crystallographic software. *J. Appl. Cryst.* **40,** *658–674*
51. Terwilliger, T. (2004) SOLVE and RESOLVE: automated structure solution, density modification, and model building. *J. Synchrotron Radiat.* **11,** 49–52
52. Emsley, P., and Cowtan, K. (2004) Coot: model-building tools for molecular graphics. *Acta Crystallogr. D Biol. Crystallogr.* **60,** 2126–2132
53. Afonine, P. V., Grosse-Kunstleve, R. W., Echols, N., Headd, J. J., Moriarty, N. W., Mustyakimov, M., Terwilliger, T. C., Urzhumtsev, A., Zwart, P. H., and Adams, P. D. (2012) Towards automated crystallographic structure refinement with phenix.refine. *Acta Crystallogr. D Biol. Crystallogr.* **68,** 352–367
54. Katoh, K., and Standley, D. M. (2013) MAFFT Multiple sequence alignment software version 7: improvements in performance and usability. *Mol. Biol. Evol.* **30,** 772–780
55. Overmars, L., Kerkhoven, R., Siezen, R. J., and Francke, C. (2013) MGcV: the microbial genomic context viewer for comparative genome analysis. *BMC Genomics* **14,** 209
56. Cantarel, B. L., Coutinho, P. M., Rancurel, C., Bernard, T., Lombard, V., and Henrissat, B. (2009) The carbohydrate-active EnZymes database (CAZy): an Expert Resource for Glycogenomics. *Nucleic Acids Res.* **37,** D233–D238